LASER & PHOTONICS REVIEWS

www.lpr-journal.org

Highly Efficient and Ultra-Broadband Yellow Emission of Lead-Free Antimony Halide toward White Light-Emitting Diodes and Visible Light Communication

*Qionghua Mo, Jiabing Yu, Chen Chen, Wensi Cai, Shuangyi Zhao, HaiYun Li, and Zhigang Zang**

Due to the broadband emission induced by self-trapped excitons (STEs), low-dimensional hybrid lead halides are regarded as an emerging class of highly efficient light emitters. However, the toxic lead element impedes their commercial application. Here, a new air-stable hybrid lead-free metal halide $[Na(DMSO)_2]_3SbBr_6$ with a 0D structure constituted by $[SbBr_6]$ octahedral and $[Na(DMSO)_2]_3$ units is synthesized at room temperature, which exhibits a high photoluminescence quantum yield of 60% and an ultra-broadband yellow emission centered at 608 nm, with a full width at half-maximum of 160 nm. First-principles calculations and experimental studies unveil that the formation of STEs in this 0D structure contributes the broad emission. Then, warm white light-emitting diodes (WLEDs) are proposed by combining blue LED chips with yellow $[Na(DMSO)_2]_3SbBr_6$, showing a color rendering index of 85, a correlated color temperature of 3603 K. Finally, the prepared WLEDs are utilized in visible light communication (VLC) with an achieved −3 dB bandwidth of 7.2 MHz and a high transmitted data rate of 81.6 Mbps by applying orthogonal frequency division multiplexing modulation with adaptive bit loading. This research not only enriches the family of perovskite related materials, but also inspires the potential of low-dimensional metal halide in VLC.

1. Introduction

Owing to the excellent optoelectronic properties, 3D lead halide perovskites have attracted substantial attention in the past few years, with applications being reported in photovoltaic cells,[1–4] light-emitting diodes (LEDs),[5–9] nano lasers,[10–14] and photodetectors (PDs).[15–18] Compared with their 3D counterparts, low-dimensional (2D/1D/0D, low-D) hybrid metal halide materials show an unique properties of ultra-broadband emission in the visible light range caused by self-trapped excitons (STEs) emission, and are therefore considered as excellent emitters for white LEDs (WLEDs).[19–21] The strong electron–phonon coupling in low-D metal halides is generally regarded to be responsible for STEs, thus lower dimensional metal halides are preferred to produce STEs emission.[22] Therefore, a series of low-dimensional hybrid materials, such as 2D [2,2″-(ethylenedioxy)-bis(ethylammonium)]$PbBr_4$[23] and (2,6-dimethylpiperazine)$_3Pb_2Br_{10}$,[24] 1D (acridine)Pb_2Cl_5,[25] (3-aminoquinoline)-$PbCl_4$,[26] $(C_4N_2H_{14})PbBr_4$, $(C_4N_2H_{14})$-$Pb_{0.987}Mn_{0.013}Br_4$,[27] (*N,N,N*″trimethylethylenediammonium)Pb_2Br_6,[28] and (trans-2,5-dimethylpiperazine)$PbBr_4$,[29] and 0D $(C_{13}H_{19}N_4)_2PbBr_4$[30] have been developed to act as photoluminescence (PL) materials. However, the existence of toxic lead ions (Pb^{2+}) may cause severe problem to environment and human body, hindering their future commercial development. Therefore, it is of great emergency to replace the toxic Pb^{2+} with nontoxic metal ions, and form lead-free metal halides with low-dimensional structures and an excellent performance.

In recent years, lead-free metal halides with nontoxic metal ions (e.g., Sn^{2+}, In^{3+}, Sb^{3+}, Mn^{2+}, Cu^{+}, etc.) and low dimensional electronic structures were synthesized and used to fabricate WLEDs.[31–35] For example, Xia et al. reported a 0D $(PMA)_3InBr_6$ single crystal (SC), which exhibited a broad orange-emitting with a PL quantum yield (PLQY) of 35%. WLEDs were then obtained by coating this orange-emitting $(PMA)_3InBr_6$, green phosphor Ba_2SiO_4:Eu^{2+} and blue phosphor $BaMgAl_{10}O_{17}$:Eu^{2+} on a commercial UV chip, showing a Commission Internationale de l´Eclairage (CIE) of (0.33,0.37), a correlated color temperature (CCT) of 5383 K.[33] Subsequently, Kanatzidis and coworkers reported a 1D (DAO)Sn_2I_6 SC with a PLQY of 20.3% and fabricated WLEDs by combining (DAO)Sn_2I_6 with a commercial UV-emitter, resulting in a CIE chromaticity coordinates of (0.55,0.42), a CCT of 1822 K, and a CRI of 75.[31] However, the excess phosphors with

Q. Mo, J. Yu, W. Cai, S. Zhao, H. Li, Z. Zang
Key Laboratory of Optoelectronic Technology and Systems (Ministry of Education)
Chongqing University
Chongqing 400044, China
E-mail: zangzg@cqu.edu.cn
C. Chen
School of Microelectronics and Communication Engineering
Chongqing University
Chongqing 400044, China

The ORCID identification number(s) for the author(s) of this article can be found under https://doi.org/10.1002/lpor.202100600

DOI: 10.1002/lpor.202100600

rare-earth components and the use of UV chip pumped low-D hybrid metal halides for WLEDs may not meet the requirement for practical applications. Hence, it inspires researchers to pay more attention on efficient lead-free metal halides, improving the optical properties of WLEDs without adding phosphors or UV chips.

In this work, we synthesized 0D lead-free $[Na(DMSO)_2]_3SbBr_6$ SCs and their nanocrystals (NCs) counterpart at room temperature, both of which exhibited a broad wide yellow PL, with a full width at half maximum of 160 nm, a stokes shift as large as 180 nm, a photoluminescent lifetime as long as ≈3 μs, and a PLQY as high as 60%. The broad wide emission of $[Na(DMSO)_2]_3SbBr_6$ is considered to be originated from STEs, which was induced by the strong electron–phonon coupling in the soft 0D crystalline structures. The prominent optical performance of $[Na(DMSO)_2]_3SbBr_6$ with yellow emission enables the achievement of efficient WLEDs by using a blue LED chip. Such WLEDs show a CRI of 85, a CCT of 3603 K, and an operating stability as long as 130 h. Meanwhile, we proposed the efficient WLEDs as the light converter in visible light communication (VLC), exhibiting a −3 dB bandwidth of 7.2 MHz and a transmit data rate up to 81.6 Mbps by way of orthogonal frequency division multiplexing (OFDM) modulation with adaptive bit loading. Our results therefore demonstrate the great potential of the lead-free $[Na(DMSO)_2]_3SbBr_6$ materials in future solid-state white light illumination and VLC.

2. Results and Discussion

$[Na(DMSO)_2]_3SbBr_6$ SCs were crystallized via an antisolvent method at atmosphere and room temperature, in which toluene as an antisolvent diffused slowly into dimethyl sulfoxide (DMSO) precursor solutions containing NaBr with $SbBr_3$ (see details in the Experimental Section). The diffused toluene in the precursor solutions might consume DMSO, acting as a good solvent for precursors and leading to an increase of precursor concentration. As a result, the precursors of NaBr with $SbBr_3$ were precipitated from the original DMSO solution and $[Na(DMSO)_2]_3SbBr_6$ SCs were formed. Similarly, the antisolvent method was used to synthesize $[Na(DMSO)_2]_3SbBr_6$ NCs. In order to obtain NCs with small sizes, oleylamine was added into the precursor to act as the stabilizer and the precursor solution needs to be added into toluene directly to accelerate the crystallinity. To evaluate the crystal structure of $[Na(DMSO)_2]_3SbBr_6$ metal halides, their samples were measured using single-crystal X-ray diffraction. The analysis revealed that the space group of $[Na(DMSO)_2]_3SbBr_6$ is an R-3 trigonal system with lattice parameters of $a = 15.391(2)$ Å, $b = 15.391(2)$ Å, and $c = 13.926(3)$ Å. More detailed crystal data are described in Table S1, Supporting Information.

The isolated $[SbBr_6]$ octahedrals are surrounded by the $[Na(DMSO)_2]_3$ units and thus form a 0D metal halide structure (**Figure 1**a,b). Detailed analysis reveal that the distance between two adjacent Sb ions is over 13.9 Å, circumventing the interactions between polyhedrons in $[Na(DMSO)_2]_3SbBr_6$. As shown in Figure 1c, the measured NC powder X-ray diffraction (PXRD) patterns matches well with the calculated ones, indicating the high purity and crystallinity of the $[Na(DMSO)_2]_3SbBr_6$ NCs.

Moreover, the bandgap structure and projected density of states (PDOS) were calculated via density functional theory (DFT), as shown in Figure 1d,e. A bandgap of 3.2 eV was found for the calculated $[Na(DMSO)_2]_3SbBr_6$, which was larger than the experimental value of 2.53 eV (Figure S1, Supporting Information). This is a due to the heavy element effect in DFT calculation. The valence band maximum (VBM) and conduction band minimum (CBM) are composed of completely flat bands, suggesting that the electronic states are highly localized due to the confined $[SbBr_6]$ octahedral.[36–39] The PDOS shows that the VBM consist of Br 4p and Sb 5s orbitals, while the CBM is constituted by Br 4p and Sb 5p orbitals. Thus we believe each of $[SbBr_6]$ octahedral separated by $[Na(DMSO)_2]_3$ units can serve as independent luminescence center.

Under an excitation of 365 nm UV light, $[Na(DMSO)_2]_3SbBr_6$ solution, NC powders and SCs exhibit a bright yellow emission with high PLQYs of 60%, 60%, and 56%, respectively (Figure 1f). The calculated absorption spectrum agrees well with the experimental data, as shown in Figure 1g, with the absorption onset located at ≈430 nm. The PL and PL excitation (PLE) spectra of the $[Na(DMSO)_2]_3SbBr_6$ NCs are shown in Figure 1h. The PLE peak shows a wide range of 345–430 nm, which are in accordance with the absorption results. A broadband PL spectrum centered at 608 nm is also found, which suggests a large Stokes shift (≈200 nm) in the $[Na(DMSO)_2]_3SbBr_6$. The rod-like SCs exhibit similar optical characteristics with $[Na(DMSO)_2]_3SbBr_6$ NCs (Figure S2, Supporting Information). In addition to the broad emission, the large Stokes shift of $[Na(DMSO)_2]_3SbBr_6$ implies a negligible self-absorption. The broad and bright yellow emission of the $[Na(DMSO)_2]_3SbBr_6$ imply their promising potentials in WLEDs. Thermogravimetric analysis of $[Na(DMSO)_2]_3SbBr_6$ NCs was also studied with a decomposing temperature of ≈393 K (Figure S3, Supporting Information). In addition, Figure S4, Supporting Information presents the PL spectra and the PLQY of $[Na(DMSO)_2]_3SbBr_6$ during the period of 35 days under ambient conditions. The luminescence intensity remains almost unchanged is shown in Figure S4a, Supporting Information. The $[Na(DMSO)_2]_3SbBr_6$ still maintain 88% of initial PLQY even after exposure in air for 35 days (see Figure S4b, Supporting Information), indicating its strong oxygen and moisture resistance. The above mentioned results clearly demonstrate the great potential of our $[Na(DMSO)_2]_3SbBr_6$ in light emitting applications.

Figure 2a presents the transmission electron microscopy (TEM) images of as-synthesized $[Na(DMSO)_2]_3SbBr_6$ NCs, which show an elliptic morphology with a mean size of ≈30 nm. To evaluate nanoscale details of the NCs, high-resolution TEM (HRTEM) was measured as shown in Figure 2b. Clear lattice fringes with an interplanar distance of 0.32 nm, corresponding to a (303) plane of $[Na(DMSO)_2]_3SbBr_6$ NCs suggesting the good crystallinity of the $[Na(DMSO)_2]_3SbBr_6$ NCs. Similarity, Figure 2c exhibits a homogeneous distribution of elements in $[Na(DMSO)_2]_3SbBr_6$ NCs, implying the negligible segregation and separation of corresponding elements. Scanning electron microscope (SEM) was used to investigate its surface morphology, from which the formation of NCs and uniform distribution of elements are demonstrated (Figure S5, Supporting Information). Figure 2d shows the Fourier transform infrared absorption (FTIR) for $[Na(DMSO)_2]_3SbBr_6$ NCs. S═O and C—S stretching vibration peaks are found in both $[Na(DMSO)_2]_3SbBr_6$ and DMSO, indicating the presence of DMSO groups in as-prepared samples. The small shifts of the two FTIR vibration patterns might be due to the bonding effects between DMSO groups and Na^+ ions,[40,41]

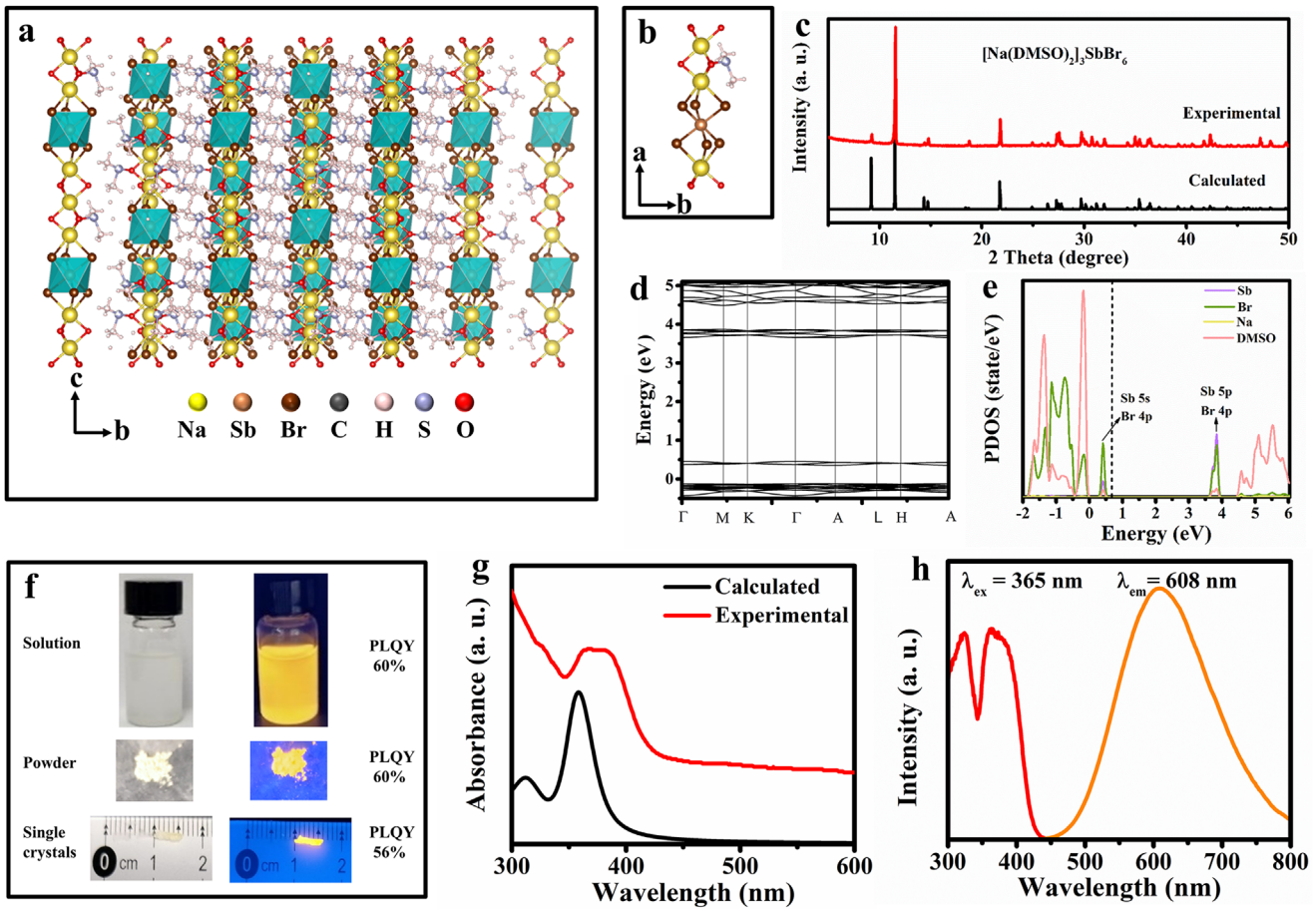

Figure 1. a) Crystal structure of $[Na(DMSO)_2]_3SbBr_6$. b) Detailed view of the crystal structure. c) PXRD and calculated XRD of $[Na(DMSO)_2]_3SbBr_6$. d) DFT electronic band structure and e) projected density of states (PDOS) of $[Na(DMSO)_2]_3SbBr_6$. f) Photographs of $[Na(DMSO)_2]_3SbBr_6$ solution, powder, and single crystals with/without UV light. g) The calculated and experimental UV–vis absorption spectra of $[Na(DMSO)_2]_3SbBr_6$ NCs. h) PLE and PL spectra of $[Na(DMSO)_2]_3SbBr_6$ NCs.

which is also in agreement with the structures (Figure 1a,b). The X-ray photoelectron spectroscopy (XPS) results in Figure 2e further confirm the existence of Na, Sb, Br, S, and O elements. The location of Na 1s peak at 1072.3 eV, Sb 3d peaks at 540.4 and 531.1 eV, Br 3d peak at 70.1 and 69.1 eV, S 2p peak at 166.9 eV, and the O 1s peak at 535.9 eV (Figure S6, Supporting Information) clearly indicate the successful synthesis of $[Na(DMSO)_2]_3SbBr_6$.

To further study the emission mechanism of the broad emission of $[Na(DMSO)_2]_3SbBr_6$ NCs, time-resolved PL (TRPL) curve was measured. As shown in **Figure 3**a, the average fitting times of the TRPL curve is 3.0 μs, which is larger than that of 3D $CsPbX_3$ perovskites with a band edge emission.[42,43] PL spectra of $[Na(DMSO)_2]_3SbBr_6$ NCs excited under different wavelength were also investigated, as shown in Figure 3b. The identical shapes and features of PL peaks are observed under variety of excitation wavelength, indicating that the emission originated from the same excited state.[44] To clarify the effects of permanent defects on the PL performance, the excitation powers were increased to see the change of PL intensity. As shown in Figure 3c, the PL intensity of $[Na(DMSO)_2]_3SbBr_6$ NCs exhibits a linear dependence on the excitation power, ruling out the effect of permanent defects on the PL (Figure S7

Supporting Information).[45] Besides, the grind of a SC into powder may result in a reduction of PLQY from 56% to 43%, further excluding the role of surface defects on the emission.[46] The Raman spectrum of the $[Na(DMSO)_2]_3SbBr_6$ perovskites was carried out, in which a symmetric stretching (A_{1g}), bending (T_{2g}), and asymmetric stretching (E_g) modes bands centered at 71, 194, and 214 cm^{-1} were found, respectively, as shown in Figure 3d. The three Raman modes can be perfectly fitted by the following Equation (1) in octahedrons:[38]

$$\nu^2_{A_{1g}} \approx \nu^2_{E_g} + \frac{3}{2}\nu^2_{T_{2g}} \quad (1)$$

It can be inferred the A_{1g}, T_{2g}, and E_g modes belong to the $[SbBr_6]$ octahedron, which further verified the strong electron-photon interaction in $[SbBr_6]$ octahedron in the $[Na(DMSO)_2]_3SbBr_6$, leading to the formation of STEs. As a result, the emissive mechanism of the $[Na(DMSO)_2]_3SbBr_6$ NCs is considered as STEs, which is well in agreement with the reported lead-free low-D metal halides.[47,48] A schematic configuration coordinate diagram is presented in Figure 3e, which shows the photo physical processes of the STE mechanism.

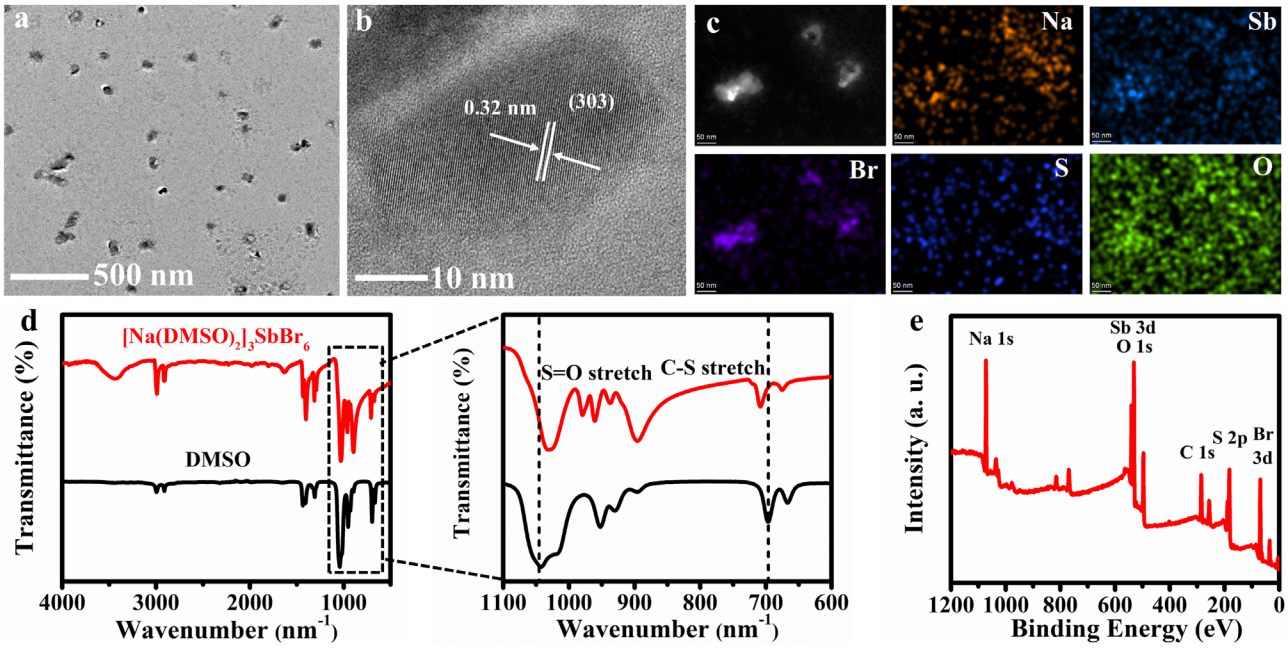

Figure 2. a) TEM and b) HRTEM images of $[Na(DMSO)_2]_3SbBr_6$ NCs. c) Element mapping measurement of $[Na(DMSO)_2]_3SbBr_6$ NCs. d) FTIR spectra and magnified spectra of FTIR of $[Na(DMSO)_2]_3SbBr_6$ NCs and DMSO. e) XPS full scan spectra of $[Na(DMSO)_2]_3SbBr_6$ NCs.

Under a high-energy excitation, electrons of ground states are excited into excited states, and then "cool" to an excited exciton energy state. Owing to the strong electron–phonon interactions resulted in the octahedrons distortion, a STE energy state can be found in the NCs, facilitating the broad emission with a large Stokes shift and a long PL decay time. As shown in Figure 3f, a uniform PL distribution of the NCs film was confirmed by PL mapping of the $[Na(DMSO)_2]_3SbBr_6$ NCs based films, which was considered as the result of the uniform size distribution of $[Na(DMSO)_2]_3SbBr_6$ NCs, consistent with the results of TEM and SEM.

To test the white light emission potentials, WLEDs were made by directly sticking the $[Na(DMSO)_2]_3SbBr_6$ onto commercial blue LED chips. **Figure 4**a depicts the PL spectrum of the obtained WLEDs at a driving voltage of 2.9 V. As shown in Figure 4b, the as-fabricated WLEDs exhibit a high CRI value of 85, an appropriate CCT value of 3603 K, and a CIE color coordinate of (0.3636, 0.2851), indicating an excellent optical performance as a white-light emitter. Figure 4c presents the evolution of PL spectra of the WLEDs with the increase of driving voltages. PL intensity enhances with the increase of driving voltages, the PL spectra peaks, and the respective CIE color coordinate remain almost unchanged as shown in Table S2, Supporting Information and Figure 4c. The operating stability of WLEDs were then studied in ambient air. The PL evolution of the yellow peak corresponding to the $[Na(DMSO)_2]_3SbBr_6$ metal halides presents only a slightly reduction of emissive intensity and a negligible PL shift, which confirms an excellent photostability of $[Na(DMSO)_2]_3SbBr_6$ under blue chip excitation (Figure 4d). As shown in Figure 4e, although the power efficiency of WLEDs decreases with the increase of operating time, the power efficiency remains ≈57% of its initial value even after being continuously operated for 130 h, suggesting the good stability of $[Na(DMSO)_2]_3SbBr_6$. Apart from power efficiency, the CRI and CCT values of WLEDs only slightly reduce, with a high value of 81 and 3097 K, respectively (Figure 4f), even after 130 h, suggesting a good operational stability of WLEDs.

As a potential solid-state light source, the fabricated WLEDs based on $[Na(DMSO)_2]_3SbBr_6$ can also serve as the light converter for VLC, as illustrated in **Figure 5**a. Figure 5b shows the measured eye diagram of the VLC system modulated by a square-wave signal with a frequency of 7 MHz, where clear and wide-open eye can be observed. With the increase of driving frequency, the electrical-optical-electrical (EOE) response of WLEDs reduces, reaching a −3 dB bandwidth of ≈7.2 MHz (Figure 5c). Although the received signal-to-noise ratio (SNR) of the VLC system is found to gradually decrease with the increase of frequency, a high SNR value of ≈20 dB could still maintain when operating the WLEDs at its −3 dB bandwidth frequency (Figure 5d). By applying OFDM modulation with adaptive bit loading, the corresponding bit loading profile is shown in Figure 5e, and the obtained constellation diagrams of 4-ary quadrature amplitude modulation (4-QAM), 8-QAM, 16-QAM, 32-QAM, 64-QAM, 128-QAM are shown in Figure 5f–k, respectively. The results suggest that the VLC system can achieve a data transfer rate as high as 81.6 Mbps, which is over 11 times the measured −3 dB bandwidth.

3. Conclusion

In this work, new 0D lead-free metal halide $[Na(DMSO)_2]_3SbBr_6$ SC and its NC counterpart are synthesized at room temperature, which exhibit not only highly efficient broad yellow emission with a high PLQY of 60%, but also a long PL decay time of (3.1 μs), suggesting that the STEs are origin of the PL mechanism. Due to the negligible self-absorption and broad emission,

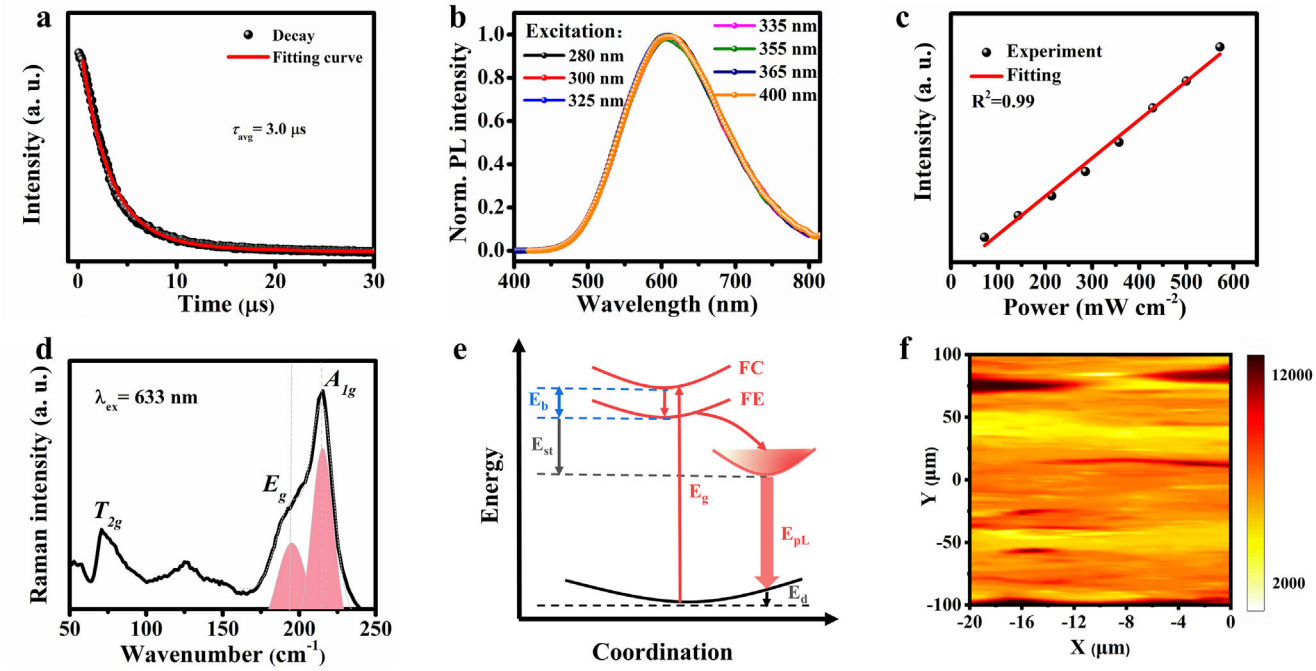

Figure 3. a) TRPL decay curve of $[Na(DMSO)_2]_3SbBr_6$ NCs at room temperature. b) PL spectra of the $[Na(DMSO)_2]_3SbBr_6$ NCs recorded at different excitation wavelengths. c) PL intensity versus excitation power for $[Na(DMSO)_2]_3SbBr_6$ NCs. The linear fitting result shows a high R^2 value of 0.99. d) Raman spectrum of $[Na(DMSO)_2]_3SbBr_6$ NCs under a 633 nm excitation. e) Illustration of relaxation mechanism for the broadband emission in $[Na(DMSO)_2]_3SbBr_6$. f) PL mapping of $[Na(DMSO)_2]_3SbBr_6$ NCs (excited at 325 nm).

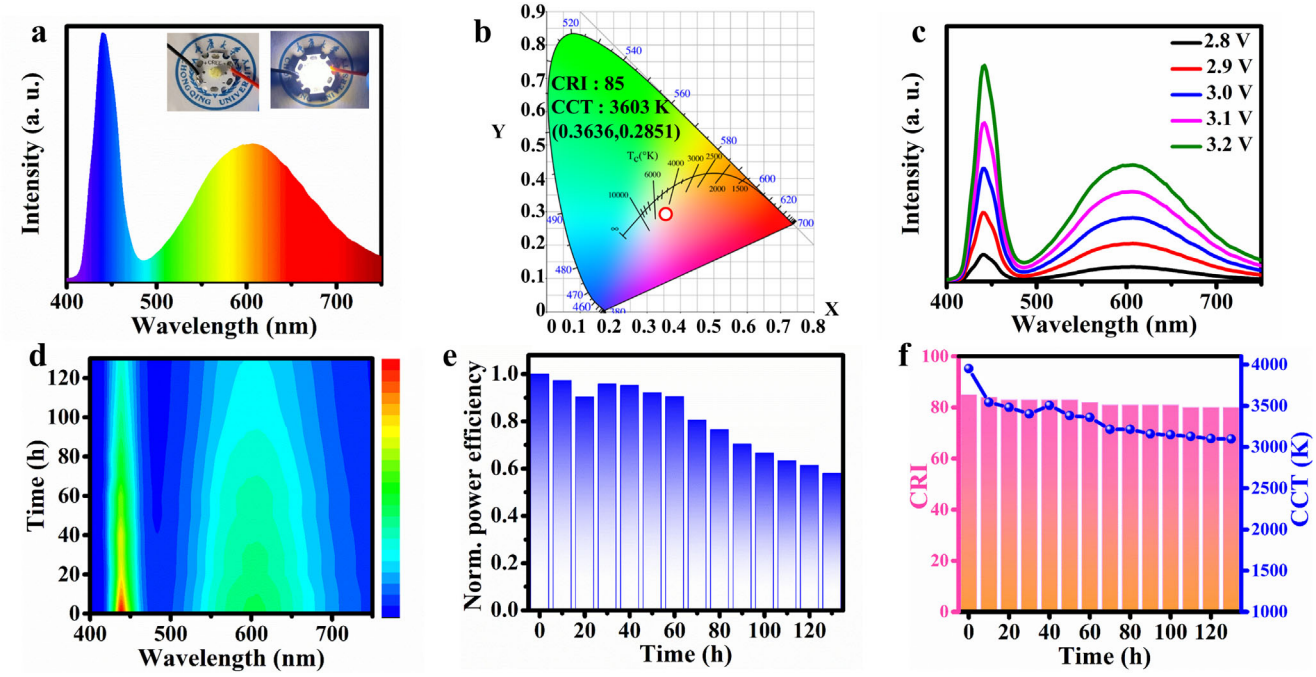

Figure 4. a) PL spectra of WLEDs based on $[Na(DMSO)_2]_3SbBr_6$. b) CIE chromaticity diagram of the WLEDs. c) PL spectra of WLEDs under different voltages. d) Contour plot of the PL spectra as a function of time and wavelength. e) The normalized power efficiency of WLEDs under operation as a function of time. f) CRI and CCT of WLEDs at different time.

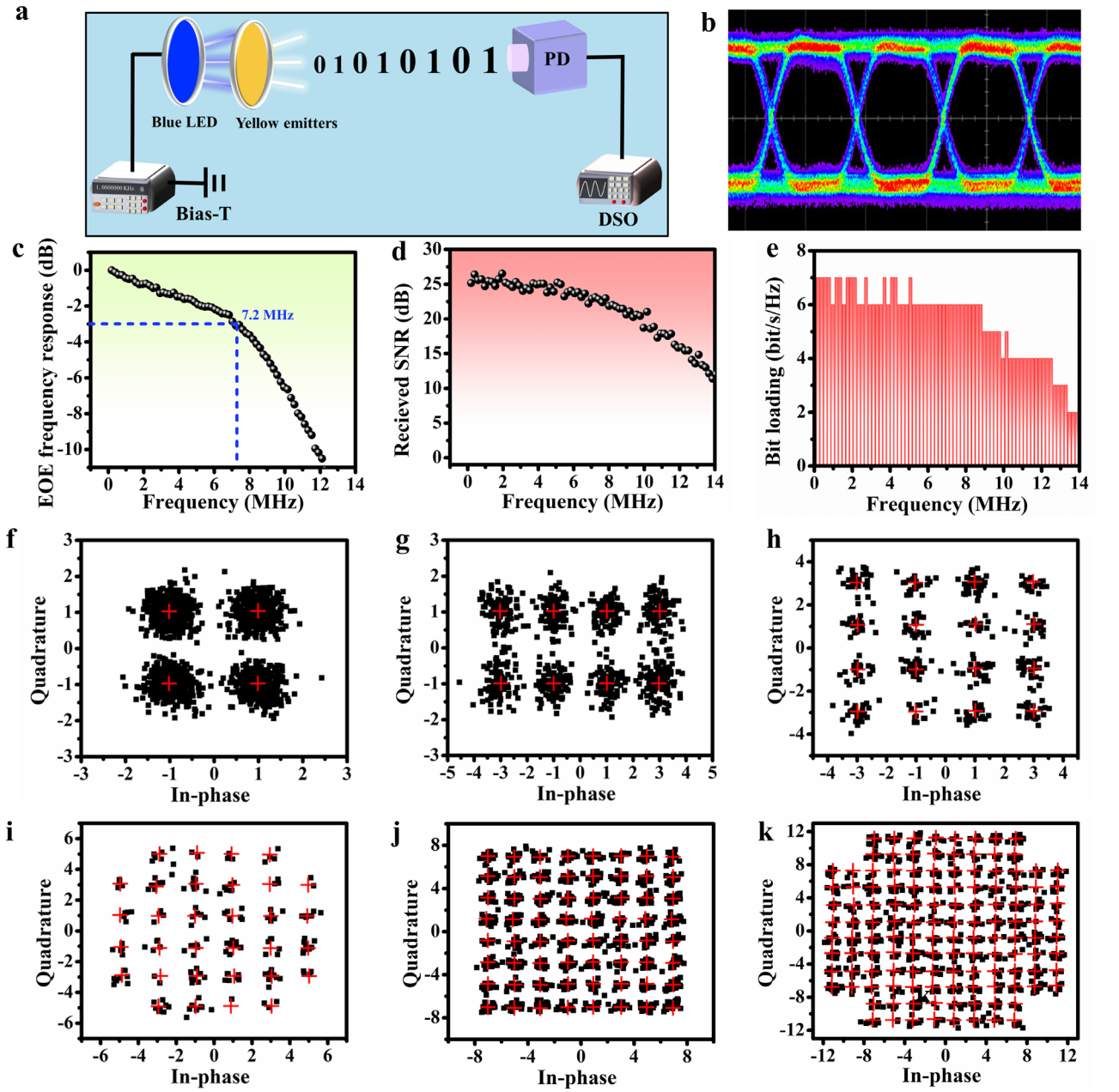

Figure 5. a) A schematic diagram of the VLC system using the fabricated WLEDs, b) the measured eye diagram at 7 MHz, c) the EOE frequency response, d) the received SNR as a function of frequency, e) the bit loading profile, and the corresponding f) 4-QAM, g) 8-QAM, h) 16-QAM, i) 32-QAM, j) 64-QAM, and k) 128-QAM constellation diagrams.

the $[Na(DMSO)_2]_3SbBr_6$ metal halides are used as an emitter for WLEDs, showing a high CRI of 85, an appropriate CCT of 3603 K, and a 130 h operating stability due to the good thermal stability. Moreover, the proposed WLEDs are utilized in VLC, showing a −3 dB bandwidth of 7.2 MHz and a high transmission data of 81.6 Mbps using OFDM modulation with adaptive bit loading. These results demonstrate the versatile nature of low-D lead-free metal halides, opening the new path for development of next-generation solid-state illumination and other optoelectronic applications.

4. Experimental Section

Materials: Sodium bromide (NaBr, 99.99%, Sigma Aldrich), antimony bromide ($SbBr_3$,99.995% Alfa Aesar), toluene (99.5%, Sigma Aldrich), and DMSO (99.9%, Adamas) were purchased and used directly.

Synthesis of $[Na(DMSO)_2]_3SbBr_6$ 0D Perovskite NCs: 0.13 mmol NaBr and 0.13 mmol $SbBr_3$ were added into 0.5 mL DMSO, followed by a stirring at room temperature for 1 h. Oleylamine (50 µL) was added into the above precursor to act as the stabilizer. Then 0.1 mL precursor solution was quickly added into toluene (5 mL) under vigorous stirring at 1000 rpm for 10 s at room temperature.

Synthesis of $[Na(DMSO)_2]_3SbBr_6$ 0D Single Crystals: 0.8 mmol NaBr and 0.8 mmol $SbBr_3$ were dissolved in 1.2 mL of DMSO, followed by a stirring for 1 h. Then the solution was filtered by a 0.22 µm filters with 0.5 mL of the filtered precursor solution being gently added into 5 mL of toluene to let stand overnight. Finally, the crystals were washed with toluene and dried. All above-mentioned experimental processes were carried out at room temperature.

Fabrication of White-Light Diodes: $[Na(DMSO)_2]_3SbBr_6$ metal halides were stick onto 420 nm commercial chips.

Characterizations: PXRD was performed on a Cu Kα radiation (XRD-6100, SHIMADZU, Japan). UV–vis absorption spectra were performed using UV–vis spectrophotometer (UV–vis: UV-1800, SHIMADZU, Japan). All the PL/PLE/PLQY/TRPL were measured by a spectrofluorometer (Edinburgh Instruments Ltd., FLS1000, UK) at room temperature. Time-resolved spectra measurements were collected using a µF2 pulsed xenon flashlamp as the excitation source with a pulse repetition rate of 100 Hz. The TRPL were recorded at a detection wavelength of 608 nm and the excitation wavelength of 365 and 420 nm for powders and crystals, respectively. TEM measurements were performed on an electron microscope (Libra 200 FE, Zeiss, Germany). SEM characterization was measured using a JEOL JSM-7800F field emission. FTIR spectra were carried out using KBr and a Nicolet iS50 FT-IR Spectrometer (Thermo Fisher Scientific, Waltham, MA, USA). XPS spectra were performed on an ESCA Lab220I-XL. The intensity-dependent PL measurement was carried out using a laser with a 375 nm output wavelength. Raman spectrum was obtained by LabRAM HR Evolution under a 633 nm excitation.

Measurement of WLEDs and Visible Light Communication: The optical properties of the fabricated WLEDs were collected by a Keithley 2400 and a PR 670. The VLC setup is shown in Figure 5a, where the AC signal was generated by an arbitrary waveform generator (Tektronix AFG31102) which was combined with a 3.8 V DC bias via a bias-T (Mini-Circuits Bias-Tee ZFBT-6GW+) to drive the WLED. A PD (Thorlabs PDA36A2) with a −3 dB bandwidth of 12 MHz was used to convert the optical signal into an electrical signal. The obtained electrical signal was sampled by a digital storage oscilloscope (LeCroy WaveSurfer 432) and further processed offline via MATLAB.

First-Principles Calculations of $[Na(DMSO)_2]_3SbBr_6$: The electronic band structure and absorption properties of $[NaDMSO_2]_3SbBr_6$ were calculated using DFT implemented on the Vienna ab initio simulation package.[49,50] Generalized gradient approximation of Perdew–Burke–Ernzerhof exchange-correlation potential was used with the projector augmented wave method.[51] The kinetic energy cutoff was set as 400 eV. The atomic structure was relaxed with $2 \times 2 \times 2$ Gamma-center k-point mesh and the atomic force criteria of 0.005 eV $Å^{-1}$.[52,53] The electronic wavefunction was self-consistently converged with energy variation criteria of 10^{-5} eV. The density of states was obtained by sampling the Brillouin zone with $6 \times 6 \times 6$ Gamma-center k-point mesh and Gaussian smearing width of 0.05 eV. The frequency-dependent dielectric function and the absorption properties were calculated using the independent particle approximation.

Supporting Information

Supporting Information is available from the Wiley Online Library or from the author.

Acknowledgements

This work was financially supported by National Natural Science Foundation of China (61904023), Key Program Science Foundation of Natural Science Foundation of Chongqing (cstc2020jcyj-jqX0028), and Fundamental Research Funds for the Central Universities (2021CDJQY-022). The authors would like to thank Chuanyao Yang (Analytical and Testing Center of Chongqing University). $[Na(DMSO)_2]_3SbBr_6$ have been deposited in the Cambridge Crystallographic Data Centre under deposition number CCDC 2164140.

Conflict of Interest

The authors declare no conflict of interest.

Data Availability Statement

The data that support the findings of this study are available from the corresponding author upon reasonable request.

Keywords

lead-free metal halide materials, visible light communication, white light emission

Received: October 22, 2021
Revised: May 27, 2022
Published online: July 3, 2022

[1] R. J. Sutton, G. E. Eperon, L. Miranda, E. S. Parrott, B. A. Kamino, J. B. Patel, M. T. Hörantner, M. B. Johnston, A. A. Haghighirad, D. T. Moore, H. J. Snaith, *Adv. Energy Mater.* **2016**, *6*, 1502458.
[2] H. Wang, S. Cao, B. Yang, H. Li, M. Wang, X. Hu, K. Sun, Z. Zang, *Sol. RRL* **2020**, *4*, 1900363.
[3] M. Wang, H. Wang, W. Li, X. Hu, K. Sun, Z. Zang, *J. Mater. Chem. A* **2019**, *7*, 26421.
[4] B. Yang, M. Wang, X. Hu, T. Zhou, Z. Zang, *Nano Energy* **2019**, *57*, 718.
[5] H. Guan, S. Zhao, H. Wang, D. Yan, M. Wang, Z. Zang, *Nano Energy* **2020**, *67*, 104279.
[6] L. Protesescu, S. Yakunin, M. I. Bodnarchuk, F. Krieg, R. Caputo, C. H. Hendon, R. X. Yang, A. Walsh, M. V. Kovalenko, *Nano Lett.* **2015**, *15*, 3692.
[7] S. Thapa, G. C. Adhikari, H. Zhu, P. Zhu, *J. Alloys Compd.* **2021**, *860*, 158501.
[8] B. Wang, S. Y. Zhang, B. Liu, J. Li, B. Cao, Z. Liu, *ACS Appl. Nano Mater.* **2020**, *3*, 3019.
[9] D. Yan, Q. Mo, S. Zhao, W. Cai, Z. Zang, *Nanoscale* **2021**, *13*, 9740.
[10] H. Dong, C. Zhang, X. Liu, J. Yao, Y. S. Zhao, *Chem. Soc. Rev.* **2020**, *49*, 951.
[11] J. Chen, W. Du, J. Shi, M. Li, Y. Wang, Q. Zhang, X. Liu, *InfoMat* **2019**, *2*, 170.
[12] S. Ghimire, L. Chouhan, Y. Takano, K. Takahashi, T. Nakamura, K.-i. Yuyama, V. Biju, *ACS Energy Lett.* **2018**, *4*, 133.
[13] Q. Mo, T. Shi, W. Cai, S. Zhao, D. Yan, J. Du, Z. Zang, *Photonics Res.* **2020**, *8*,1605.
[14] D. Yan, T. Shi, Z. Zang, T. Zhou, Z. Liu, Z. Zhang, J. Du, Y. Leng, X. Tang, *Small* **2019**, *15*, e1901173.
[15] C. Li, C. Han, Y. Zhang, Z. Zang, M. Wang, X. Tang, J. Du, *Sol. Energy Mater. Sol. Cells* **2017**, *172*, 341.
[16] P. Ramasamy, D. H. Lim, B. Kim, S. H. Lee, M. S. Lee, J. S. Lee, *Chem. Commun.* **2016**, *52*, 2067.
[17] T. Zhang, F. Wang, P. Zhang, Y. Wang, H. Chen, J. Li, J. Wu, L. Chen, Z. D. Chen, S. Li, *Nanoscale* **2019**, *11*, 2871.
[18] H. Wang, P. Zhang, Z. Zang, *Appl. Phys. Lett.* **2020**, *116*, 162103.
[19] C. Sun, Y.-D. Yue, W.-F. Zhang, X.-Y. Sun, Y. Du, H.-M. Pan, Y.-Y. Ma, Y.-C. He, *CrystEngComm* **2020**, *22*, 1480.
[20] Y. Wang, S. Guo, H. Luo, C. Zhou, H. Lin, X. Ma, Q. Hu, M. H. Du, B. Ma, W. Yang, X. Lu, *J. Am. Chem. Soc.* **2020**, *142*, 16001.
[21] A. Biswas, R. Bakthavatsalam, S. R. Shaikh, A. Shinde, A. Lohar, S. Jena, R. G. Gonnade, J. Kundu, *Chem. Mater.* **2019**, *31*, 2253.
[22] H. Lin, C. Zhou, Y. Tian, T. Siegrist, B. Ma, *ACS Energy Lett.* **2017**, *3*, 54.

[23] E. R. Dohner, A. Jaffe, L. R. Bradshaw, H. I. Karunadasa, *J. Am. Chem. Soc.* **2014**, *136*, 13154.
[24] L. Mao, P. Guo, M. Kepenekian, I. Hadar, C. Katan, J. Even, R. D. Schaller, C. C. Stoumpos, M. G. Kanatzidis, *J. Am. Chem. Soc.* **2018**, *140*, 13078.
[25] X. Yang, L. F. Ma, D. Yan, *Chem. Sci.* **2019**, *10*, 4567.
[26] H. Barkaoui, H. Abid, A. Yangui, S. Triki, K. Boukheddaden, Y. Abid, *J. Phys. Chem. C* **2018**, *122*, 24253.
[27] Z. Yuan, C. Zhou, Y. Tian, Y. Shu, J. Messier, J. C. Wang, L. J. van de Burgt, K. Kountouriotis, Y. Xin, E. Holt, K. Schanze, R. Clark, T. Siegrist, B. Ma, *Nat. Commun.* **2017**, *8*, 14051.
[28] H. Lin, C. Zhou, J. Neu, Y. Zhou, D. Han, S. Chen, M. Worku, M. Chaaban, S. Lee, E. Berkwits, T. Siegrist, M. H. Du, B. Ma, *Adv. Opt. Mater.* **2019**, *7*, 1801474.
[29] R. Gautier, F. Massuyeau, G. Galnon, M. Paris, *Adv. Mater.* **2019**, *31*, e1807383.
[30] H. Lin, C. Zhou, M. Chaaban, L.-J. Xu, Y. Zhou, J. Neu, M. Worku, E. Berkwits, Q. He, S. Lee, X. Lin, T. Siegrist, M.-H. Du, B. Ma, *ACS Mater. Lett.* **2019**, *1*, 594.
[31] I. Spanopoulos, I. Hadar, W. Ke, P. Guo, S. Sidhik, M. Kepenekian, J. Even, A. D. Mohite, R. D. Schaller, M. G. Kanatzidis, *J. Am. Chem. Soc.* **2020**, *142*, 9028.
[32] Z. Li, Y. Li, P. Liang, T. Zhou, L. Wang, R.-J. Xie, *Chem. Mater.* **2019**, *31*, 9363.
[33] D. Chen, S. Hao, G. Zhou, C. Deng, Q. Liu, S. Ma, C. Wolverton, J. Zhao, Z. Xia, *Inorg. Chem.* **2019**, *58*, 15602.
[34] T. Jiang, W. Ma, H. Zhang, Y. Tian, G. Lin, W. Xiao, X. Yu, J. Qiu, X. Xu, Y. Yang, D. Ju, *Adv. Funct. Mater.* **2021**, *31*, 2009973.
[35] L. Wang, H. Sun, C. Sun, D. Xu, J. Tao, T. Wei, Z. H. Zhang, Y. Zhang, Z. Wang, W. Bi, *Dalton Trans.* **2021**, *50*, 2766.
[36] H. Peng, S. Yao, Y. Guo, R. Zhi, X. Wang, F. Ge, Y. Tian, J. Wang, B. Zou, *J. Phys. Chem. Lett.* **2020**, *11*, 4703.
[37] J. P. Perdew, M. Levy, *Phys. Rev. Lett.* **1983**, *51*, 1884.
[38] L. Zhou, J. F. Liao, Z. G. Huang, J. H. Wei, X. D. Wang, H. Y. Chen, D. B. Kuang, *Angew. Chem., Int. Ed. Engl.* **2019**, *58*, 15435.
[39] R. Zhang, X. Mao, Y. Yang, S. Yang, W. Zhao, T. Wumaier, D. Wei, W. Deng, K. Han, *Angew. Chem., Int. Ed. Engl.* **2019**, *58*, 2725.
[40] D. N. Minh, J. Kim, J. Hyon, J. H. Sim, H. H. Sowlih, C. Seo, J. Nam, S. Eom, S. Suk, S. Lee, E. Kim, Y. Kang, *Chem. Mater.* **2017**, *29*, 5713.
[41] N. Ahn, D. Y. Son, I. H. Jang, S. M. Kang, M. Choi, N. G. Park, *J. Am. Chem. Soc.* **2015**, *137*, 8696.
[42] W. Lv, L. Li, M. Xu, J. Hong, X. Tang, L. Xu, Y. Wu, R. Zhu, R. Chen, W. Huang, *Adv. Mater.* **2019**, *31*, e1900682.
[43] Q. A. Akkerman, G. Rainò, M. V. Kovalenko, L. Manna, *Nat. Mater.* **2018**, *17*, 394.
[44] J. Luo, X. Wang, S. Li, J. Liu, Y. Guo, G. Niu, L. Yao, Y. Fu, L. Gao, Q. Dong, C. Zhao, M. Leng, F. Ma, W. Liang, L. Wang, S. Jin, J. Han, L. Zhang, J. Etheridge, J. Wang, Y. Yan, E. H. Sargent, J. Tang, *Nature* **2018**, *563*, 541.
[45] H. Chen, J. M. Pina, F. Yuan, A. Johnston, D. Ma, B. Chen, Z. Li, A. Dumont, X. Li, Y. Liu, S. Hoogland, Z. Zajacz, Z. Lu, E. H. Sargent, *J. Phys. Chem. Lett.* **2020**, *11*, 4326.
[46] L. Zhou, J. F. Liao, Z. G. Huang, J. H. Wei, X. D. Wang, W. G. Li, H. Y. Chen, D. B. Kuang, C. Y. Su, *Angew. Chem., Int. Ed. Engl.* **2019**, *58*, 5277.
[47] S. Zhao, Q. Mo, W. Cai, H. Wang, Z. Zang, *Photonics Res.* **2021**, *9*, 187.
[48] V. Morad, Y. Shynkarenko, S. Yakunin, A. Brumberg, R. D. Schaller, M. V. Kovalenko, *J. Am. Chem. Soc.* **2019**, *141*, 9764.
[49] G. Kresse, J. Furthmüller, *Comp. Mater. Sci.* **1996**, *6*, 15.
[50] G. Kresse, J. Furthmüller, *Phys. Rev. B* **1996**, *54*, 11169.
[51] G. Kresse, D. Joubert, *Phys. Rev. B* **1999**, *59*, 1758.
[52] H. J. Monkhorst, J. D. Pack, *Phys. Rev. B* **1976**, *13*, 5188.
[53] S. Grimme, *J. Comput. Chem.* **2006**, *27*, 1787.